Review

Modeling Tracer Kinetics in Dynamic Gd-DTPA MR Imaging

Paul S. Tofts, BA(Oxon), DPhil

Three major models (from Tofts, Larsson, and Brix) for collecting and analyzing dynamic MRI gadolinium-diethylenetriamine penta-acetic acid (Gd-DTPA) data are examined. All models use compartments representing the blood plasma and the abnormal extravascular extracellular space (EES), and they are intercompatible. All measure combinations of three parameters: (1) k^{PS_p} is the influx volume transfer constant (min^{-1}), or permeability surface area product per unit volume of tissue, between plasma and EES; (2) v_e is the volume of EES space per unit volume of tissue ($0 < v_e < 1$); and (3) k_{ep}, the efflux rate constant (min^{-1}), is the ratio of the first two parameters ($k_{ep} = k^{PS_p}/v_e$). The ratio k_{ep} is the simplest to measure, requiring only signal linearity with Gd tracer concentration or, alternatively, a measurement of T1 before injection of Gd (T_{1o}). To measure the physiologic parameters k^{PS_p} and v_e separately requires knowledge of T_{1o} and of the tissue relaxivity R_1 ($\approx$ in vitro value).

Index terms: Gd-DTPA • Dynamic MRI • Tracer kinetics • Permeability • Extravascular extracellular space • Rate constant

JMRI 1997; 7:91–101

Abbreviations: EPI = echoplanar imaging, EES = extravascular extracellular space, Gd-DTPA = gadolinium-diethylenetriamine penta-acetic acid, MTGA = multiple time graphical analysis, PET = positron emission tomography, PS = permeability and surface area product.

From the NMR Unit, Institute of Neurology, Queen Square, London WC1N 3BG, England. Received and accepted November 6, 1996. Address reprint requests to P.S.T.

THERE IS INCREASING USE of dynamic MRI to characterize abnormal capillary leakage, eg, in multiple sclerosis, brain tumors, retinal disease, and breast tumors. There is a confusing plethora of approaches that differ in three principle ways:

1. The data collection procedure varies (eg, is the plasma concentration measured or not; is a bolus or infusion injection used; what MRI sequence is used?).
2. Both the presentation of theoretical models and which kinetic parameters are extracted vary. Several parameters are reported, without their equivalence, if any, being obvious. Many models are heuristic, with no relationship to the underlying physiology; these are not considered further. It will be shown that most meaningful models give parameters that are equivalent to either (a) the influx volume transfer constant (k^{PS_p}) or permeability surface area product per unit volume; (b) the extravascular extracellular space (EES) (v_e); or (c) their ratio, the efflux rate constant (k_{ep}).
3. The names and symbols used to describe these parameters vary. In this review, a set of standard symbols have been defined (Table 1). It is hoped that some of these might be adopted by the research community to facilitate intercomparisons between measurements made at different sites. In describing a particular piece of work, the authors' original equations are given but using the standard symbols to make the similarities and differences between major models more apparent. In places, the variables are labeled with a superscript to denote their use by particular authors (eg, A^B A^H used by Brix and Hoffmann and colleagues—see section on Brix et al Model).

The aim of this review is to reconcile the various models and to show the relationship (if any) to physiologic variables. Armed with this review, the reader can critically assess publications related to dynamic gadolinium-diethylenetriamine penta-acetic acid (Gd-DTPA) MRI. With appropriate MRI technique, these physiologic variables (k^{PS_p}, v_e, and k_{ep}) can be measured with good absolute accuracy, providing a result independent of the particular observer, MRI sequence, scanner, or site used. These can then be used to study normal physiology (in cases where the blood capillary is permeable) and disease progression and its response to therapy.

The review focuses on Gd-DTPA tracer; however the tracer kinetic principles can be applied to other tracers (eg, blood pool agents [1,2]), provided an appropriate plasma curve $C_p(t)$ is used, although different imaging strategies might be appropriate, since the requirements for temporal resolution are lower. Initial applications were in multiple sclerosis lesions, followed by the retina; more recent applications are in high permeability tumors, where some questions still remain concerning the effects

Table 1
Standard Set of Symbols

Symbol	Explanation	Units
A_i	Amplitude for plasma curve (Equation [3])	mM or mmole liter^{-1}
C_p	Tracer concentration in blood plasma	mM or mmole liter^{-1}
C_e	Tracer concentration in extravascular extracellular space (EES)	mM or mmole liter^{-1}
C_t	Tracer concentration in tissue ($C_t = v_e C_e + v_p C_p$)	mM or mmole liter^{-1}
F	Blood flow per unit time, per unit tissue mass	ml min^{-1} g^{-1}
Hct	Hematocrit	None
k^{PS_p}	Volume transfer constant or permeability surface area product per unit volume of tissue between EES and plasma (assumed same in each direction); 'transfer constant' or 'permeability' for short	min^{-1}
$k_{in}^{PS_p}$	Influx volume transfer constant (into EES from plasma)	min^{-1}
$k_{out}^{PS_p}$	Efflux volume transfer constant (out of EES into plasma)	min^{-1}
k_{pe}	Influx rate constant from plasma to EES; 'rate constant' for short	min^{-1}
k_{ep}	Efflux rate constant from EES to plasma	min^{-1}
m_i	Rate constant for plasma curve (Equation [3])	min^{-1}
P (P_{in} P_{out})	Permeability constant (into or out of EES)	cm min^{-1}
PS	Permeability surface area product per unit mass of tissue	cm^3 min^{-1} g^{-1}
R_1	T1 relaxivity (increase in 1/T1 per unit concentration of Gd)	sec^{-1} mM^{-1}
S	Surface area per unit mass of tissue	cm^3 g^{-1}
T_{10}	Native T1 (ie T1 of tissue before injection of Gd tracer)	sec
v_e	EES volume per unit volume of tissue	None
v_p	Blood plasma volume per unit volume of tissue	None
ρ	Density of tissue	g cm^{-3}

Note.—EES = extravascular extracellular space (or interstitial water space) in abnormal tissue.

of incomplete mixing in the early phase after injection and of flow-limited leakage.

The mixing phase, during which the injected bolus is mixing into the blood plasma and other closely coupled compartments, lasts up to about 2 minutes. Bolus tracking during this phase has been used to measure blood volume, using T2*- or T1-weighted sequences (3,4). This phase cannot be described properly using compartmental analysis and is not considered in this review. However, if the local arterial input function (ie, plasma concentration) can be measured, it may be possible to characterize leakage in the surrounding tissue during this early phase.

Early Models

Early work in tracer kinetics, before the advent of noninvasive in vivo imaging, was carried by physiologists using radioactive tracers in animals that were then killed to measure the tracer concentration in the tissue of interest (5). The application of diffusion theory to the transport of tracers across a capillary wall and the knowledge that the flux (flow rate) is proportional to the concentration gradient led to the notion of a *permeability constant P* (6,7), defined as the flux (mmole sec^{-1} or mmole min^{-1}) per unit concentration difference and per unit area of semipermeable membrane:

$$\text{flow of tracer} = P\ S\ \Delta C\ M_t \qquad (1)$$

where S is the area of the membrane per unit mass of tissue (cm^2 g^{-1}), ΔC is the concentration difference (mmole cm^{-3}) across the membrane, and M_t is the mass of the tissue concerned. (The total area of the membrane is thus S M_t.) The units of P are therefore cm min^{-1} (or cm sec^{-1}). Since S is usually unknown, physiologists often report the product of permeability and surface area per unit mass of tissue (7) (the 'PS product'; cm^3 min^{-1} g^{-1} or cm^3 sec^{-1} g^{-1}).

In early animal investigations, the PS product of permeable capillary beds was found by injecting tracer into the arterial blood supply, using either an infusion (7) or a bolus (8). The proportion of tracer that left the bloodstream and entered the tissue in one pass of blood through the capillary bed was called the 'extraction fraction' E and is related to PS by:

$$E = 1 - e^{-PS/F} \qquad (2)$$

where F is the capillary blood flow per unit mass of tissue (ml min^{-1} g^{-1}). Backflux into the capillary was ignored (ie, the extravascular concentration remained low). If the permeability is high enough to extract most of the tracer in one pass, then the extraction fraction is close to unity (PS»F, E≈1) and PS cannot be determined (since transport across the membrane is then flow limited and independent of PS). The venous concentration is then considerably less than the arterial concentration, and the concept of a well-mixed plasma compartment does not apply. On the other hand, if extraction is low, the flow is sufficient to replace tracer lost by transport through the capillary wall and the blood plasma compartment has a well-defined concentration. PS is then equal to EF (if F»PS, E≈PS/F).

In 1978, Ohno, Pettigrew, and Rapoport, at Baltimore and Bethesda (9), published a two-compartment model for the distribution of ^{14}C-labeled compounds of low molecular weight between the plasma and the brain in rats after a bolus injection. This has all the essential elements of later MRI-based models, although the later MRI workers were probably unaware of this work at the time. A dimensionally corrected version of their equations is presented here. The plasma concentration (C_p) was represented as the sum of n decaying exponentials (typically three), which were determined from blood samples:

$$C_p(t) = \sum_{i=1}^{n} A_i\ e^{-m_i t} \qquad (3)$$

The tracer uptake in the EES in unit mass of tissue is (taking account of backflux and assuming PS«F, and that the plasma volume is small):

$$\frac{dC_t}{dt} = PS\ \rho \left(C_p - \frac{C_t}{v_e} \right) \qquad (4)$$

where C_t is the tissue concentration, ρ the tissue density,

and v_e the EES per unit volume of tissue. In this equation, the extracellular concentration $C_e = C_t/v_e$, and the concentration difference C_p-C_e is driving transport of tracer across the capillary wall. The term *'extravascular* extracellular space' (also called the 'interstitial water space') is used here to specifically exclude the blood plasma space (which is technically part of the whole extracellular space). (Note that some workers have referred to the EES as the 'extracellular space', even though the latter technically includes the blood plasma.) The solution to the differential Equation (4) for the tissue concentration is:

$$C_t(t) = PS\,\rho \sum_{i=1}^{n} A_i \frac{e^{-(PS\rho/v_e)t} - e^{-m_i t}}{m_i - (PS\rho/v_e)} \qquad (5)$$

and measured values were fitted to this model on a PDP10 computer (Digital Equipment Corporation (DEC), MA) to obtain $PS\rho$ and v_e. At early times (when backflux can be ignored),

$$PS = \frac{C_t}{\rho \int_0^t C_p(t')\,dt'} \qquad (6)$$

Note that these authors (and several others) have confused themselves by measuring tissue concentration per unit mass, whereas blood concentration was per unit volume. As a result, their original versions of Equations (4–6) are dimensionally incorrect (they assumed the tissue density ρ is dimensionless and equal to 1) and physically incorrect for any density other than 1 g ml^{-1}. In this review, all concentrations are measured per unit volume, since MRI is sensitive to the amount of tracer per *voxel* (whereas in early animal experiments, the amount of tracer in a known *mass* of excised tissue was measured). Flow (F), PS product (P), and surface area (S) are still defined per unit mass for consistency with previous published physiologic work.

In 1983, Patlak et al. (10) published a generalized analysis of tracer compartments and a graphical method (multiple time graphical analysis [MTGA]) for determining PS from the initial uptake portion of the curve; this has the benefit of not requiring computer fitting. However backflux is ignored (the flux is considered unidirectional) and only the early part of the enhancement curve can be used. There is a danger of underestimating PS (depending on whether data collection continues into the period when the tissue concentration has risen high enough to produce significant backflux into the capillary). This method was used in MRI studies of rat gliomas (11-13). Their measurements of "blood-to-tissue transport constant K_i" are PS values in units of ml kg^{-1} min^{-1}. Ianotti et al (14) developed a similar method for application to positron emission tomography (PET) measurements.

Ott et al (15a) published a general expression in 1991 for leakage of ^{68}Ga-EDTA in brain tumors, which takes account of backflux and of tracer in the plasma:

$$C_t(t) = \rho\,K_1\,(1 - v_p/(1 - Hct)) \int_0^t C_p(t')e^{-k_2(t-t')}\,dt' + v_p\,C_p(t) \qquad (7)$$

(the original equation has been corrected for dimensional errors related to ρ). k_2 is called the "outflux constant"; v_p is the plasma volume ($0<v_p<1$). Estimates of K_1 and v_p were determined from the early part of the curve, whereas extending data collection beyond 40 minutes enabled k_2 to be determined. Hawkins et al (15b) published a similar expression before Ott, including the presentation of the tissue concentration as the convolution of the plasma concentration with an exponential decay impulse response. However, the work is focused around PET measurements, and an apparent error in the dimensional treatment makes it inapplicable to MRI. Yeung (16) used a similar expression for CT measurements of K_1 and v_p in brain tumors.

General Assumptions in any Model

All of the models described here make some basic assumptions related to concepts in tracer kinetics and NMR theory. These include the following (10):

1. *Compartments* exist that contain the well-mixed tracer in a uniform concentration throughout the compartment.
2. *Linear intercompartment flux*, ie, the flux between compartments is proportional to the difference in the concentrations in the two compartments.
3. *Time invariance*, ie, the parameters describing the compartments are constant during the time that data are acquired.
4. *Blood plasma* compartment, with tracer concentration C_p (units mM or mmole $liter^{-1}$)
5. A lesion *EES* compartment, with tracer concentration C_e and volume v_e per unit volume of tissue. This is the space in abnormal tissue to which leaking Gd-DTPA tracer has access and is distinct from the normal extracellular space distributed throughout the body. Strictly speaking, this space into which Gd-DTPA tracer can leak might include spaces other than the EES (eg, intracellular space), although there is no evidence of this. Throughout, it is assumed that tracer in the EES has arrived directly from a nearby capillary; however diffusion through the EES from more distant capillaries is possible and (if present) would render the simple modeling invalid. A simple calculation of the maximum possible size of the effect shows that if diffusion were as free as in pure water (ie, diffusion coefficient $D = 3 \times 10^{-5}$ cm^2sec^{-1}) and if the EES space were large (ie, little hinderance from cells), then in 10 minutes the root mean square distance traveled would be 3 mm. Microscopic circulation within the EES could increase this effect.
6. *constant relaxivity*, ie, the increase in NMR T1 relaxation rate is proportional to the concentration of Gd-DTPA tracer:

$$\frac{1}{T_1} = \frac{1}{T_{10}} + R_1\,C_t \qquad (8)$$

where C_t is the tissue concentration, R_1 is the relaxivity, and T_{10} is the 'native' T1 (ie, the value of T1 before injection of any tracer).

7. *fast exchange* of all mobile (NMR visible) protons within the tissue so that the tissue relaxes with a single T1 value, even though the Gd-DTPA is not evenly distributed but concentrated in the EES and the plasma. Although this condition appears true for exchange between cellular and extracellular spaces, the exchange between the vascular and extravascular spaces is probably not fast (17). Thus, when modeling the contribution of Gd-DTPA in the plasma, and particularly when using blood pool agents, errors may arise. The ULSTIR sequence (18) partly overcomes this problem by measuring the longitudinal magnetization in the first 40 msec after inversion, before exchange

Table 2
Comparison of Models

	Tofts and Kermode (26)	Larsson et al (25)	Brix et al (27)
Plasma concentration	Assumed normal (biexponential)	Measured from blood samples	Fitted with single rate constant
Gd-DTPA injection	Bolus	Bolus	Infusion
Estimated parameters	"k" = $k^{PS\rho}$ "v_1" = v_e	"EF/v" ≈ $k_{ep} = k^{PS\rho}/v_e$	"k_{21}" = $k_{ep} = k^{PS\rho}/v_e$ "A" = A^B "k_{el}" ≈ m_1
Assumed signal proportional to concentration?	No	Not necessarily	Yes
Is T_{10} needed?	Yes	Not necessarily	No
Is in vivo R_1 needed?	Yes	No	No
Can initial rise be used?	Yes (for $k^{PS\rho}$)	No	No

becomes appreciable. More accurate values of plasma volume are then obtained.

• MODELING MRI DATA

The advent of the clinical use of Gd-DTPA in Japan and Europe from the mid-1980s to probe breakdown in the blood-brain barrier in multiple sclerosis and tumors brought about a flurry of new work studying the dynamics of Gd enhancement. In 1986, Yoshida et al (19) measured T1 at a range of times after injection, both in plasma and in brain tumors, but there was no pharmacokinetic or physiologic modeling of the data. Three European groups started modeling the signal enhancement as a function of time. These models all apparently developed independently within about 2 years of each other; each had distinct approaches to both data collection and modeling and each spawned rich veins of applications that are still being exploited now. The locations were in London (Tofts and Kermode), Copenhagen (Larsson and coworkers), and Heidelberg (Brix and coworkers).

In February 1989, at the seventh annual meeting of the Society for Magnetic Resonance Imaging in Los Angeles, Tofts and Kermode presented a poster on their new model (20). In a rapidly enhancing multiple sclerosis lesion in brain white matter (reaching its peak at 10 minutes), an influx volume transfer constant (loosely referred to as 'permeability':$k^{PS\rho}$) of 0.056 min^{-1} and an EES (v_e) of 0.18 were measured. A more slowly enhancing lesion (peak at 45 minutes) had lower permeability ($k^{PS\rho}$ = 0.012 min^{-1}) and larger EES (v_e = 0.41). These data were included in a published letter (21). Later that year (in August 1989), it was shown at the Society of Magnetic Resonance in Medicine in Amsterdam (22). At the same meeting, Larsson et al showed their model (23), reporting rate constants k_{ep} in acute multiple sclerosis in the range of 0.04–0.11 min^{-1}, compatible with those of Tofts and Kermode (24). Larsson et al published their full paper on modeling dynamic Gd-DTPA MRI data in 1990 (25) (submitted in April 1989), followed by Tofts and Kermode in 1991 (26) (submitted in June 1989). Brix et al presented their model in New York in 1990 (26a), and publication followed in 1991 (27).

Table 2 provides a comparison of models.

Tofts and Kermode (26) Model

In the original formulation (20-22,26,28), the permeability P was assumed to be isodirectional (ie, the same in both directions), which is the case for simple diffusive transport. In this case, the flux of tracer from the plasma into the EES compartment is given by Equation (1). However, it is conceivable that there are different permeability constants P_{in} and P_{out} for flux into and out of the EES (eg, if there were active transport mechanisms or differences in diffusion, viscosity, or pressure on each side of the membrane); these are used here for generality. In addition, the treatment is extended here to include the contribution of tracer in the blood plasma to the total tissue concentration. Although this is small (ie, $v_p \approx 0$) in blood-brain barrier lesions, it is often significant in tumors. The flux of tracer into the abnormal EES is then (see Equation [1]):

$$v_e V_t \frac{dC_e}{dt} = (P_{in} C_p - P_{out} C_e) S M_t \qquad (9)$$

where V_t and M_t are the volume and mass of tissue being considered (and hence $v_e V_t$ is the volume of EES in that tissue, and the total area is $S M_t$). The differential equation describing the tissue concentration is then

$$\frac{dC_t}{dt} - v_p \frac{dC_p}{dt} = k_{in}^{PS\rho} C_p - \left(\frac{k_{out}^{PS\rho}}{v_e}\right)(C_t - v_p C_p) \qquad (10)$$

(Note that $C_t = v_e C_e + v_p C_p$). The *volume* transfer constant $k^{PS\rho}$ has the simple physiologic meaning of being the PS product multiplied by the tissue density (ρ) (ie, $k^{PS\rho} = PS\rho$) or the permeability surface area product per unit *volume* of tissue ($k^{PS\rho} = P.SM_t/V_t = PS\rho$). It is given this name to distinguish it from the transfer constant K_t, which is the permeability surface area product per unit *mass* of tissue ($K_t = PS$). It is labeled 'PSρ' to emphasize that it is the PS per unit volume of tissue and to distinguish it from the rate constants k_{ep}, k_{21}, for example. Under the conditions of small plasma volume ($v_p \approx 0$) and isodirectional permeability (ie, $k_{in}^{PS\rho} = k_{out}^{PS\rho}$), this differential equation describing tracer flux is essentially identical to that of Ohno et al (9) (Equation [4]).

The plasma concentration after the injection of a bolus of Gd-DTPA was assumed to be that measured in normal control subjects by Weinmann (29). This was fitted to a biexponential decay (see Fig 1), which is expected from the compartmental theory:

$$C_p(t) = D \sum_{i=1}^{2} a_i^T e^{-m_i t} \qquad (11)$$

where D is the dose (mmole/kg), and amplitudes a^T are normalized for unit dose (so that C_p is then known for any size dose). The fitted values were a_1^T = 3.99 kg/liter, a_2^T = 4.78 kg/liter, m_1 = 0.144 min^{-1}, m_2 = 0.0111 min^{-1}. Using this plasma concentration, and solving Equation (10), gives the tissue concentration:

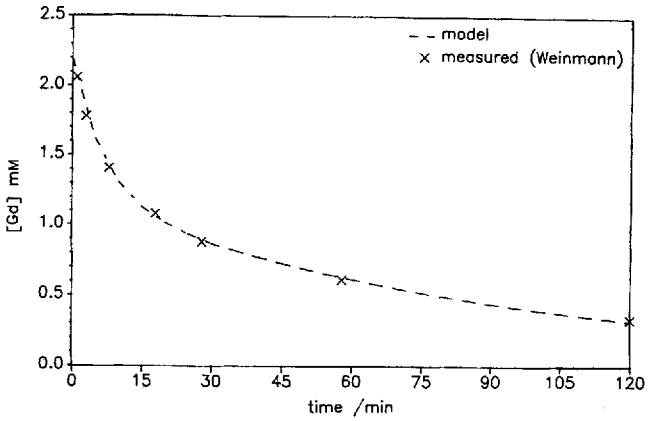

Figure 1. Plasma concentration after a bolus of 0.25 mmole/kg of Gd-DTPA, measured in normal control subjects from blood samples by Weinmann (29) and modeled by the sum of two exponentials (from Tofts and Kermode [26]).

$$C_t(t) = D\,k_{in}^{PS\rho}\sum_{i=1}^{2} a_i^T \frac{e^{-(k_{out}^{PS\rho}/v_e)t} - e^{-m_i t}}{m_i - (k_{out}^{PS\rho}/v_e)} + v_p D \sum_{i=1}^{2} a_i^T e^{-m_i t} \quad (12)$$

The native T1 of the tissue was measured using a relaxed spin echo and an inversion recovery sequence. Repeated inversion recovery sequences were then run after bolus injection of Gd-DTPA. A straightforward theoretical expression for the signal enhancement (ie, the increase in signal divided by the signal before injection) is a function of the sequence timing parameters (TR, TI, TE) and T_{10} (which are known), the tissue relaxivity R_1 (which was assumed to be equal to that in water) and the tissue concentration (which is the only unknown). Values of $k^{PS\rho}$ and v_e (originally called k and v_i) were estimated (assuming that $k_{out}^{PS\rho} = k_{in}^{PS\rho}$, ie, $P_{in} = P_{out}$, and ignoring plasma volume, ie, $v_p = 0$) with a least-squares fitting program, using Equation (12) and the expression for signal enhancement (see Fig 2). First, note (from Equation [12]) that $k_{out}^{PS\rho}$ cannot be determined independently and, secondly, that v_e can only be determined by assuming $k_{out}^{PS\rho} = k_{in}^{PS\rho}$. This equation is essentially identical to that of Ohno et al (9) for isodirectional permeability and $v_p = 0$ (Equation [5]).

In later work, the model was extended in several ways. The initial slope of the signal time curve, before the tissue concentration has risen high enough to cause significant backflux, is proportional to the permeability (26,30) (eg, see Equations [6, 9]). The T1 weighting of the sequence signal S can be defined by the time parameter T_k as follows:

$$T_k = \frac{1}{S}\frac{\partial S}{\partial(1/T_1)} = \frac{\partial E}{\partial(1/T_1)} \quad (13)$$

where E is the enhancement (the fractional increase in signal). For a spin echo sequence, $T_k \approx T_{10}$. The signal enhancement at short times, before the plasma concentration has had time to decrease, is then given by:

$$E = \frac{S(t)}{S(0)} - 1 = R_1 T_k C_t = R_1 T_k C_p(0)\,[k_{in}^{PS\rho} t + v_p] \quad (14)$$

where $C_p(0)$ is the plasma concentration immediately after bolus injection, and the v_p term has been added in this review. Thus, the permeability can in principle be determined from the initial slope.

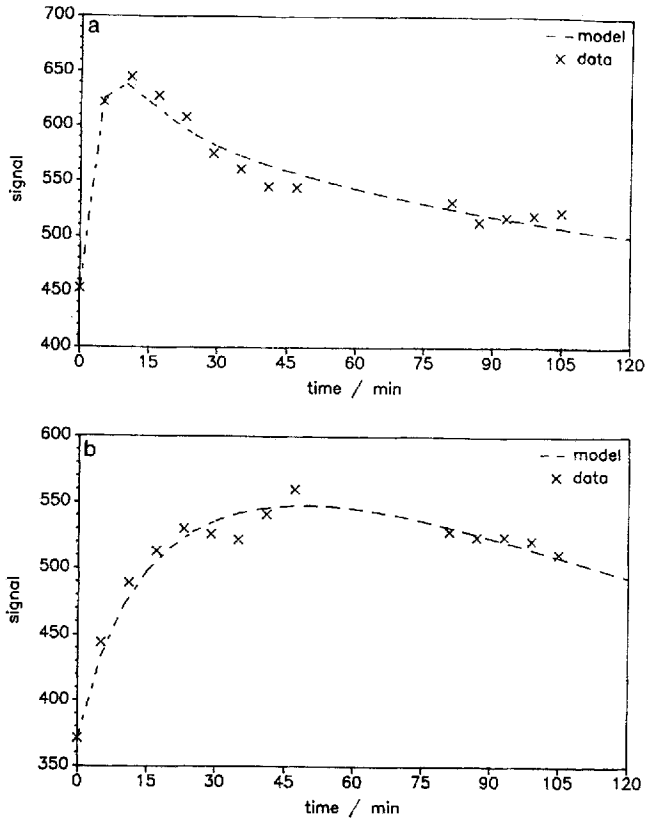

Figure 2. Gd-DTPA enhancement curves in a rapidly enhancing, acute, multiple sclerosis lesion (upper) and a slowly enhancing, chronic lesion (lower) using an inversion recovery (IR1020/40/500; TR/TE/TI) sequence. The upper curve represents $k^{PS\rho} = 0.050\ min^{-1}$, $v_e = 0.21$; the lower curve represents $k^{PS\rho} = 0.013\ min^{-1}$, $v_e = 0.49$. The native T1 was estimated from normal white matter (from Tofts and Kermode [26]).

The model was applied to leaking capillaries in the retina using spin echo data (31,32). The method for permeability measurement was validated by extracting the vitreous and measuring the amount of Gd-DTPA that had leaked from the retina into the vitreous (31). A comparison of bolus and infusion injections (33) showed that the bolus is usually more efficient at achieving a particular tissue concentration (the exception might be for a short infusion time and a high rate constant $k_{out}^{PS\rho}/v_e$). The model fits well to gradient echo data from human breast tumors (34) and to data from implanted human breast tumors (35). Predictions were made of the increased sensitivity to low permeability blood-brain barrier lesions that could be achieved using delayed imaging (up to 2 hours after injection) and repetition time and gradient echo tip angle were optimized (36).

The model has been criticized for its assumption of normal plasma concentration $C_p(t)$. If $C_p(t)$ is known for the particular subject, this knowledge can be used by fitting $C_p(t)$ to the sum of exponentials to determine the plasma parameters a^T_i and m_i (Equation [11]). Alternatively, if C_p is described numerically, a more general solution to the first-order differential Equation (10) is (37):

$$C_t(t) = k_{in}^{PS\rho}\int_0^t C_p(t')e^{-(k_{out}^{PS\rho}/v_e)(t-t')}\,dt' + v_p C_p(t) \quad (15)$$

similar to the expression of Ott (Equation [7]).

Larsson et al. (25) Model

Using the extraction fraction concept of Renkin and Crone (see Equation [2]), a differential equation for the tracer flux was obtained, similar to that of Ohno (Equation [5]), except with PS replaced by EF. If the capillary flow is sufficiently high (ie, if F»PS), then EF = PS and this is identical to Equation (5). The plasma concentration after injection of a bolus of Gd-DTPA was measured for each patient by taking a series of blood samples and measuring the amount of tracer in each sample (using neutron activation) and fitted to the sum of three exponentials (see Equation [3]).

Two approaches were used to model the signal as a function of Gd concentration. In the simple one, the signal was assumed to be linearly related to Gd concentration; then the signal is related to the permeability by:

$$S(t) = S(0) + \frac{\dot{S}\,(t)}{\sum_{i=1}^{3} A_i} \sum_{i=1}^{3} \frac{A_i\,(e^{-(EF\rho/v_e)t} - e^{-m_i t})}{m_i - EF\rho/v_e} \qquad (16)$$

where $\dot{S}$ is the initial slope of the signal. The measured signal S(t) was fitted to this expression with only $EF\rho/v_e$ and $\dot{S}$ as free parameters. In the more complex approach, the native T1 was measured (before injection of Gd) and the relaxation rate R_1^L (= 1/T1) calculated from the signal at each time point. No assumption was made regarding signal linearity. The relaxation rate is given by:

$$R^L(t) = R^L(0) + \frac{\dot{R}^L(t)}{\sum_{i=1}^{3} A_i} \sum_{i=1}^{3} \frac{A_i\,(e^{-(EF\rho/v_e)t} - e^{-m_i t})}{m_i - EF\rho/v_e} \qquad (17)$$

where $\dot{R}$ is the initial slope of the curve. The measured relaxation rate $R^L(t)$ was fitted to this expression with $EF\rho/v_e$ and $\dot{R}$ as free parameters. Note that the initial slope has been used to 'calibrate' the system so that the relaxivity R_1 is not needed. Nor is the native T1 (ie, T_{10}) needed in the simple approach (both T_{10} and R_1 were needed in the Tofts and Kermode model). However, the price paid is the loss of $k^{PS\rho}$ (or equivalently $EF\rho$); only the ratio of $EF\rho$ to v_e is found. These Equations (16) and (17) to determine the rate constant $EF\rho/v_e$ are comparable with Ohno's Equation (5). In a separate presentation (38), Larsson and coworkers used an in vitro value of relaxivity R_1 and a measurement of T_{10} in their model to determine both $k^{PS\rho}$ and v_e separately.

Myocardial perfusion (ie, blood flow F) was assessed from the dynamic Gd-DTPA uptake in the myocardium (39-42). The quantity EF is measured for transport from arterial blood (rather than plasma, as previously) to the EES. If the extraction fraction E is known from animal studies, F can be inferred. High values of EF (about 0.5 ml min^{-1} g^{-1}) were observed; assuming a normal value of E (50%), plausible values of flow F (1.0 ml min^{-1} g^{-1}) can be inferred. However, E is a sensitive function of flow F (Equation [2]), and if flow were abnormally low, E would probably be increased. In rats, Burstein et al (43) concluded that image enhancement was limited by diffusion into the EES (ie, by PS) and independent of blood flow (ie, F»PS and EF = PS).

The arterial input function (ie, plasma concentration) in the descending aorta was measured in real time (39-41) using an ECG-gated inversion recovery (IR) prepared fast gradient echo sequence (128 × 128 matrix; TR = 6.5; TI = 15 msec–10 seconds). It was also measured from blood samples using ^{99m}Tc-DTPA labeling, which confirmed the MRI measurements. A dramatic mixing effect was seen. In the first 35 seconds after bolus injection into a brachial vein (which took less than 10 seconds), the plasma concentration was raised up to three times that expected from simple multiexponential decay (see Figs 1 and 3). Venous concentrations did not reach arterial values for about 2 minutes (39).

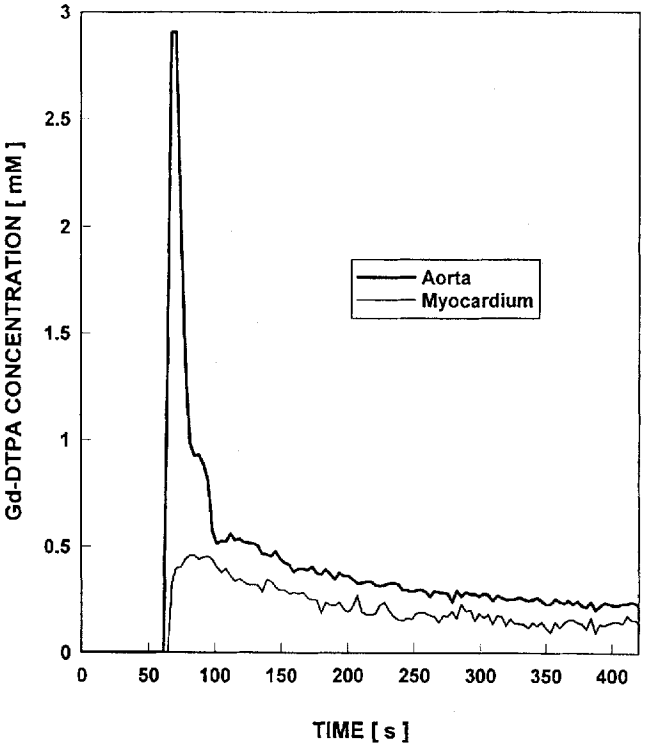

Figure 3. Plasma concentration in the first 6 minutes after a bolus injection of 0.1 mmole/kg of Gd-DTPA, measured using an IR-FLASH sequence. Note the initial spike in aortic concentration (from Larsson et al [40]).

Brix et al Model (26a,27)

The flux of Gd-DTPA tracer from the plasma (compartment 1) into the EES (compartment 2) is:

$$\frac{dM_2}{dt} = k_{12}\,M_1 - k_{21}\,M_2 \qquad (18)$$

where M_1 and M_2 are the total amounts of Gd-DTPA in the plasma and the EES, respectively. Setting $M_1 = C_p V_1$ and $M_2 = C_e V_2$, where V_1 and V_2 are the total volumes of the plasma and EES, respectively, using $V_1 = v_p V_t$; $V_2 = v_e V_t$, and comparing with Equation (9), we see the rate constants k are related to the forward and backward permeabilities (P_{in}, P_{out}) by:

$$k_{12} = k_{pe} = \frac{P_{in}\,S\rho}{v_p} = \frac{k_{in}^{PS\rho}}{v_p};$$
$$k_{21} = k_{ep} = \frac{P_{out}\,S\rho}{v_e} = \frac{k_{out}^{PS\rho}}{v_e} \qquad (19)$$

where the plasma and EES compartments have been relabeled 'p' and 'e', respectively.

Weinmann's data on the plasma concentration after injection of a bolus of Gd-DTPA (29) were felt to be sufficiently well described during the first 20 minutes by a single exponential decay; first-order elimination from the plasma compartment was therefore used, characterized by a rate constant k_{el}. The actual injection procedure

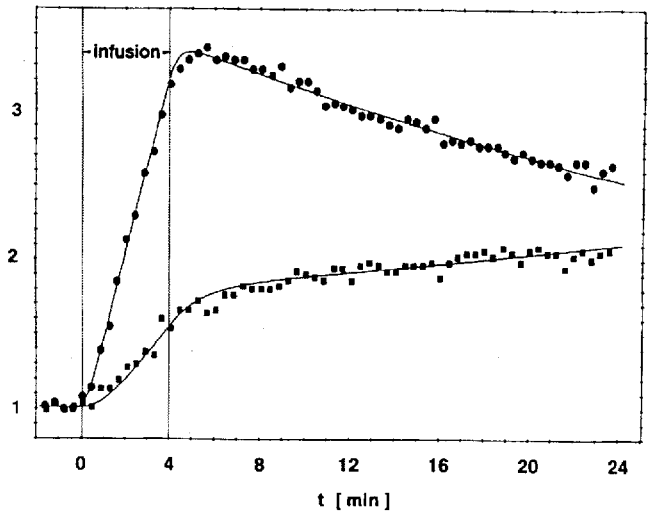

Figure 4. Signal enhancement in two parts of a brain tumor during and after a 4-minute infusion. The upper curve represents $A^B = 2.54$, $k_{ep} = 2.59\ min^{-1}$, $k_{el} = 0.024\ min^{-1}$; the lower curve represents $A^B = 0.82$, $k_{ep} = 0.73\ min^{-1}$, $k_{el} = -0.016\ min^{-1}$ (from Brix et al [27]).

used was a constant rate infusion (typically for 4 minutes), since this could be given in a more controlled way than a bolus. Data collection started just before the start of the infusion and continued after it had ended. An example is shown in Figure 4; the lower curve is still rising after 20 minutes (giving a negative value of k_{el}); the authors state (27) that this may be caused by transport of tracer from neighboring parts of the heterogeneous lesion and that k_{ep} is not affected because it is estimated from the wash-in phase of the curve.

The signal enhancement for the SE100/10 sequence was assumed to be proportional to the concentration of Gd-DTPA in the tissue. The signal is at any time t is then

$$\frac{S(t)}{S(0)} = 1 + \frac{A^B}{k_{el}-k_{ep}}\left(\frac{ce^{k_{ep}t'}-1)e^{-k_{ep}t}}{k_{ep}} - \frac{(e^{k_{el}t'}-1)e^{-k_{el}t}}{k_{el}}\right) \quad (20)$$

where $t' = t$ during the infusion, $t' = \tau$ (the duration of the infusion) after the infusion, and A^B is an arbitrary constant. The authors point out that "It is a remarkable property that ... the shape of the temporal response S(t)/S(0) is determined ... only by the kinetic parameters k_{21} [ie, k_{ep}] and k_{el}." The measured signal S(t) was fitted to this expression with A^B, k_{ep}, and k_{el} as free parameters (see Fig 4).

Note that the 'calibration' of the system is contained in the constant A^B so that once again, as in the Larsson model, the relaxivity R_1 and the native T1 are not needed, and only the rate constant k_{ep} ($= k_{out}^{PS_p}/v_e$) is found. The plasma curve was not assumed normal (as did Tofts), nor was it measured directly (as did Larsson), but instead its clearance rate was estimated from the measured tissue curve.

After a bolus (ie, $k_{ep}\tau \ll 1$, $k_{el}\tau \ll 1$), this expression reduces to:

$$\frac{S(t)}{S(0)} = 1 + A^B\tau\left(\frac{e^{-k_{ep}t}-e^{-k_{el}t}}{k_{el}-k_{ep}}\right) \quad (21)$$

which is equivalent to the previous equations of Ohno, Tofts, and Larsson (Equations [5, 12, 16, 17]).

More recently, Hoffmann et al, from the Heidelberg group, have used a fast T1-weighted gradient echo sequence and a reduced infusion length of 1 minute (45). A slightly modified equation was used with a redefined constant A (here called A^H). After a bolus injection, the equation reduces to:

$$\frac{S(t)}{S(0)} = 1 + A^H k_{ep}\left(\frac{e^{-k_{ep}t}-e^{-k_{el}t}}{k_{el}-k_{ep}}\right) \quad (22)$$

Parameter maps of A^H (as well as k_{ep}) were considered diagnostic, so it is of interest to know the physical significance of A^H. Shortly after a bolus injection, the enhancement $(S(t)/S(0)-1)$ is $A^H k_{ep} t$ and using the previous expression for the initial slope (Equation [14]), we see that:

$$A^H \approx R_1 T_k C_p(0)\ v_e \quad (23)$$

Thus, A^H approximately corresponds to the size of the EES, if the relaxivity, the native T1, and the dose do not vary significantly. Using a similar approach, the original A^B of Brix (Equation [20]) has the approximate value $A^B \approx R_1 T_k C_p(0) k^{PS_p}/\tau$, ie, corresponding to the permeability (provided the relaxivity, T_{10}, and dose procedure do not alter).

Other Work

Buckley et al (46) adapted the Brix model to fit data from breast tumors. k_{12} and k_{21} were relabeled k_{in} and k_{out}, respectively. After a bolus injection, a fast T1-weighted gradient echo (TR = 12 msec; 128 × 256 matrix) was used. The time between injection and the start of data collection were fitted as free parameters. They pointed out that mixing of the bolus is facilitated by using a saline flush.

Shames et al (2) recorded the signal from tumors, a large blood vessel (the inferior vena cava), and an oil calibration phantom after injection of a blood pool marker (albumin-Gd-DTPA). Using the assumption of signal linearity with Gd concentration, and a public-domain pharmacokinetic modeling computer program, they measured PS and the tissue plasma volume v_p (47).

Su et al (48a) published a model in 1994 following the same principles as previous workers. A calibration curve was generated using a phantom to convert signal enhancement ratio to Gd concentration; as discussed in the Assumptions section, this curve would be in error since the tissue will have different T_{10} from the phantom.

Gowland et al (48b) studied brain tumors using echo-planar imaging (EPI). The first passage of the bolus could be observed. Blood samples were taken to measure the plasma concentration. The efflux time constant (ie, $1/k_{ep}$) was estimated.

Flickinger et al (49) reported that in breast tumors, the most specific finding for separating benign from malignant lesions was the ratio of maximum intensity change to the time interval for this to be reached. Interestingly, this ratio is approximately equal to the initial slope of the enhancement curve, and thus approximately proportional to $k_{in}^{PS_p}$ (Equation [14]). On the other hand, Heiberg et al (50) reported that the peak enhancement has high specificity. For a rapidly enhancing tumor ($k_{ep} \gg m_1$), using Equations (11) and (12), the maximum tissue concentration $C_t^{max} \approx (v_e + v_p)C_p(0)$ and thus gives a good indication of the tumor extracellular space (the sum of the intra- and extravascular components). Therefore, workers may find heuristic tissue enhancement parameters that give

valuable information, without having related them to changes in the underlying physiologic parameters.

• DISCUSSION

Assumptions

The additional assumptions made by some of the MRI workers are discussed here in more detail.

The *plasma clearance parameters* A_i and m_i are required to characterize the lesion from the tissue concentration. The simplest procedure is to assume they are normal (as Tofts did). The magnitudes of the errors arising from this assumption are still not known, although there has been some theoretical discussion (26,34). There is now a great need to make systematic measurements of plasma clearance curves in control subjects and patients to determine the inter- and intrasubject variability (arising from both physiologic effects and injection procedure) and to determine how this variability propagates into errors in the lesion parameters. In rapidly enhancing lesions, the initial spike in the plasma concentration (39-41) is likely to be important (51) (see Fig 3).

The second option is to measure the plasma concentration. Initially, sequential blood samples were taken (15a,16,25), although this is inconvenient and impractical in a clinical situation. More recently, MRI has been used to observe a major blood vessel (2,18,39-41,47,48b,52). Ideally, this should be the vessel that is directly supplying the tissue of interest; however this requires that a MRI slice can be placed through this vessel; in practice this may be too far removed from the lesion to be imaged simultaneously with it. Some organs may not derive their supply from a single vessel (eg, the breast). Imaging a remote major vessel (eg, the aorta) may give sufficient information, although there may be considerable mixing and dilution of the bolus after being sampled before it reaches the leaking capillary.

The third option, used by Brix, is to estimate the plasma clearance from the tissue curve by including its clearance rate as a free parameter in fitting the enhancement curve, although this prevents k^{PS_p} from being estimated. This extra degree of freedom may increase the uncertainty in k_{ep}; the fitting may be ill-conditioned if the lesion efflux rate constant is low enough to approach the plasma clearance constant ($k_{ep} \approx k_{el}$ in Equations [20–22]), and there may a problem in distinguishing k_{ep} from k_{el} since the equations are symmetric with respect to interchange of these two fitted variables.

Blood pool contrast agents are much more stable in their concentration, and relatively simple methods may be used to determine their concentration.

The *low extraction assumption* (see Equation [2]), ie, that flow is sufficient to replace tracer lost from the capillary by leakage (F»PS), is true for permeabilities up to about $k^{PS_p} = 0.1$ min^{-1} (since typical blood flow is F = 1 ml min^{-1} g^{-1}) and holds for multiple sclerosis lesions (26) and retinal lesions. Tumors and the myocardium may have apparent values of k^{PS_p} up to 1 min^{-1}(27,34,36,45). Here the extraction is significant, and the tracer flux may be flow limited. In this case, an 'apparent permeability' has been measured, which Larsson et al (25) have shown is equal to EF (see Larsson et al Model section and Equation [16]). Although it is a combination of permeability and flow (see Equation [2]), it is still a physiologic quantity, independent of the MR method used to measure it. By measuring flow F separately (see Other Physiologic Parameters section), it is possible that true PS could be estimated (provided the extraction E does not approach 1).

The *in vivo relaxivity* R_1 has been assumed to be equal to the in vitro value (ie, that in aqueous solution), although the in vitro value can, in principle, be altered in the tissue environment by factors such as temperature, viscosity, binding, reduced water content, and water compartmentalization. The determination of the rate constant (k_{ep}) is independent of R_1; however k^{PS_p} will be wrongly estimated if R_1 alters from its assumed value. From the linear equation relating signal enhancement and permeability (Equation [14]), it is seen that it is approximately the product ($R_1 k^{PS_p}$) that is determined. It is unlikely that it will ever be possible to measure the in vivo R_1 value in the particular lesion of interest, and currently there is no option but to assume a value for R_1 if the permeability is to be estimated. Measurements in vivo in animals in tumors (53), heart tissue (54), and liver (55) give R_1 values close to in vitro values, suggesting that the assumption is reasonable.

Signal or enhancement linearity with Gd concentration has been assumed by several workers (2,25,27,45,48a). Here the concept is explored in more detail, using a spin echo sequence as an example. The signal from a T1-weighted spin echo, at low concentrations, is

$$\begin{aligned} S(C) &= g\ PD\ (1 - e^{-TR(T_{10}^{-1} + R_1 C)}) \\ &\approx S(0) + g\ PD\ TR\ e^{-TR/T_{10}}\ R_1 C \qquad (TR\ R_1 C \ll 1) \\ &\approx S(0) + g\ PD\ TR\ R_1 C \qquad (TR\ R_1 C \ll 1,\ TR \ll T_{10}) \end{aligned} \tag{24}$$

where C is the concentration (in tissue or a phantom), g is the instrument gain, PD is the proton density, and a Taylor expansion in $x = TR\ R_1\ C$ has been used. The signal enhancement (ie, fractional increase in signal) is then:

$$\begin{aligned} E(C) = \frac{S(C) - S(0)}{S(0)} &\approx \frac{TR\ e^{-TR/T_{10}}}{(1 - e^{-TR/T_{10}})} R_1 C \quad (TR\ R_1 C \ll 1) \\ &\approx R_1 T_{10} C \qquad (TR\ R_1 C \ll 1,\ TR \ll T_{10}) \end{aligned} \tag{25}$$

Thus the *signal* increases linearly with concentration, and provided we are on the linear part of the signal versus 1/T1 curve (ie, $TR \ll T_{10}$), the constant of proportionality (g PD TR R_1) is independent of T_{10}, although it does depend on the material slightly through PD (and perhaps R_1). In contrast, the enhancement has a constant of proportionality ($R_1 T_{10}$ at small TR) that depends very much on the material. For this reason systems that involve calibration of signal *enhancement* versus concentration using phantoms are fundamentally flawed.

The dependence of signal on Gd-DTPA concentration can be determined using Ni-DTPA doped gels with tissue-like T1 and T2 values (56). Gd-DTPA added to this substrate has the same relaxivity as in vitro. (In contrast, adding Gd-DTPA to aqueous solutions of Mn++ or Cu++ ions gives an altered relaxivity because they bind to excess DTPA.)

The more complete treatment of *nonlinear signal dependence on T1* (and hence on Gd concentration) is not without pitfalls. A theoretically correct analytic expression for the signal is easily produced; however the system may be nonideal, particularly in having a distribution of tip angles across the slice, which reduces the accuracy of this expression. T1 measurements made using these same expressions can be wildly inaccurate, or very good, depending principally on the slice profile and tip angle accuracy; the same considerations apply to the determination of Gd concentration, even though T1 may not determined explicitly. Ideally, the theoretical expression

should be confirmed with phantoms of known Gd concentration or T1 values.

Choice of a Model and a Method

Comparing the equations for tissue concentration for Tofts, Larsson, and Brix (Equations [12, 16, 17, 21 ,22]) we can see that all three groups are estimating *the same efflux rate constant*

$$k_{ep} = \frac{k_{out}^{PS}}{v_e} = \frac{EF_P}{v_e} = k_{21} \qquad (26)$$

The actual estimates obtained will differ in the three methods because the plasma concentration is handled differently.

The *optimum injection protocol* is still open to discussion; however it is likely to be of duration 60 seconds or less (33,45). Most workers have used bolus injections, since these give useful qualitative information used by radiologists. If the duration is more than about 10 seconds, the *center* of the injection should be considered the time of the bolus. If enhancement is rapid, the exact time of injection should probably be a fitted parameter (46); otherwise variable and uncontrolled lag times between injection and imaging may be an extra source of variation in the apparent fitted parameters.

The *T1-weighted sequence* may be a spin echo, gradient echo (2D or 3D), IR-prepared fast gradient echo, or EPI. The choice will depend on what sequences are available, the time resolution and spatial coverage required, and whether sensitivity to low Gd concentrations is required.

The *plasma clearance parameters* A_i and m_i can be determined in three possible ways (see Assumptions section). MRI measurement in a large vessel is probably the most satisfactory, if it is practically possible.

If a *simple analysis* is required, k^{PS_P} can be estimated from the slope of the initial linear portion of the enhancement curve, using Equation (14). T_{10} can be measured or a normal value assumed. There is no need for nonlinear least-squares curve fitting. The duration of this initial linear portion may be very short (too short to use, as in rapidly enhancing tumors (34)) or can last 10s of minutes (as in retinal lesions (31,32).

Following the enhancement curve into the nonlinear time portion enables the *efflux rate constant* k_{ep} (= k^{PS_P}/v_e) to be measured (Equations [5, 12, 16, 17, 20, 21, 22]). If the signal increase with concentration is nonlinear, T_{10} must be measured and used with a theoretical expression for the signal as a function of concentration S(C) in the T1-weighted sequence. Alternatively, calibration phantoms give an approximate relationship for S(C) (Equation [24]).

If data from the nonlinear time portion have been collected, they can be used to estimate the *influx transfer constant* $k_{in}^{PS_P}$ (Equation [12]). T_{10} is measured or (less satisfactorily) a normal value assumed. The estimate can be refined by improving the knowledge of T_{10} and the T1 weighting of the sequence. The *extravascular extracellular space* v_e can also be estimated (since k_{ep} is already available and assuming the permeability is the same in each direction). Since the EES (v_e) can vary with edema, the transfer constant k^{PS_P} provides a physiologically more relevant measure of the state of the capillary permeability than does the efflux rate constant k_{ep} (= k^{PS_P}/v_e).

The *fitting procedure* should determine all the free parameters in a single operation so that all the measured signals are equally weighted and noise is propagated correctly.

Other Physiologic Parameters

This review has concentrated on two physiologic parameters that can be determined from analysis of tracer uptake curves: permeability and EES. However, in addition to the native T1, there are two more that can often be obtained in the same MRI examination (making use of the Gd-DTPA bolus) that are particularly relevant if tumors (with increased vascularity) are being characterized and that may add to the physiologic specificity of the examination.

First, the plasma volume (v_p) (or blood volume) can be determined, either by including a v_pC_p term in the tissue concentration (2,47) (see Equations [7, 12, 15]), if the tissue is sufficiently well vascularized that the contribution from this term is large enough to be determined with good precision. Alternatively, blood volume can be determined by Gd-DTPA bolus tracking (3,4) using the same bolus that is later to be used to estimate permeability and EES. The size of the plasma space v_p may possibly predict the capillary surface area S, thus perhaps allowing permeability P to be estimated (rather than just the PS product). For example the quantity (PS/v_p) might be relatively independent of S and v_p.

Second, the blood flow (F) can be estimated from the transit time of the Gd-DTPA bolus. Alternatively, a separate sequence using arterial spin labeling techniques (which do not require the use of an exogenous tracer) can be used to measure flow. Other MR measurements (PD, T2, magnetization transfer, diffusion, and spectroscopy) may also add to the specificity of the examination.

• CONCLUSIONS

With appropriately good techniques of MRI data collection and tracer modeling of the images, physiologic variables can be measured in an objective, reproducible, and noninvasive way. These will have a role in understanding disease process, testing patients in the clinic, and evaluating the effectiveness of new treatments.

Acknowledgments: I am grateful to Bruce Berkowitz, Gunnar Brix, David Buckley, Henrik Larsson, Geoff Parker, Tim Roberts, David Shames, and Mike Wendland for reviewing an earlier version of this review. The NMR Research Unit is generously supported by the Multiple Sclerosis Society of Great Britain and Northern Ireland.

References

1. van Hecke P, Marchal G, Bosmans H, et al. NMR imaging study of the pharmacodynamics of polylysine-gadolinium-DTPA in the rabbit and the rat. Magn Reson Imaging 1991; 9:313–321.
2. Shames DM, Kuwatsuru R, Vexler V, Muhler A, Brasch R. Measurement of capillary permeability to macromolecules by dynamic magnetic resonance imaging: a quantitative noninvasive technique. Magn Reson Med 1993; 29:616–622.
3. Edelman RR, Mattle HP, Atkinson DJ, et al. Cerebral blood flow: assessment with dynamic contrast-enhanced T2*-weighted MR imaging at 1.5T. Radiology 1990; 176:211–220.
4. Hacklander T, Reichenbach JR, Hofer M, Modder U. Measurement of cerebral blood volume via the relaxing effect of low-dose gadopentetate dimeglumine during bolus transit. AJNR Am J Neuroradiol 1996; 17:821–830.
5. Fenstermacher JD, Blasberg RG, Patlak CS. Methods for quantifying the transport of drugs across brain barrier systems. Pharmacol Ther 1981; 14:217–248.
6. Pappenheimer JR. Passage of molecules through capillary walls. Physiol Rev 1953; 33:387–423.
7. Renkin EM. Transport of potassium-42 from blood to tissue in isolated mammalian skeletal muscles. Am J Physiol 1959; 197: 1205–1210.
8. Crone C. The permeability of capillaries in various organs as determined by use of the 'indicator diffusion' method. Acta Physiol Scand 1963; 58:292–305.
9. Ohno K, Pettigrew KD, Rapoport SI. Lower limits of cerebrovascular permeability to nonelectrolytes in the conscious rat. Am J Physiol 1978; 235:H299–307.

10. Patlak CS, Blasberg RG, Fenstermacher JD. Graphical evaluation of blood-to-brain transfer constants from multiple-time uptake data. J Cereb Blood Flow Metab 1983; 3:1–7.
11. Kenny J, Schmiedl U, Maravilla K, Starr F, Graham M, Spence A, Nelson J. Measurement of blood-brain barrier permeability in a tumor model using magnetic resonance imaging with gadolinium-DTPA. Magn Reson Med 1992; 27:68–75.
12. Schmiedl U, Kenny J, Maravilla K. Kinetics of pathologic blood-brain barrier permeability in a astrocytic glioma using contrast-enhanced MR. AJNR Am J Neuroradiol 1992; 13:5–14.
13. Krueck WG, Schmiedl UP, Maravilla KR, Spence AM, Starr FL, Kenny J. MR assessment of radiation-induced blood-brain barrier permeability changes in a rat glioma model. AJNR Am J Neuroradiol 1994; 15:625–632.
14. Iannotti F, Fieschi C, Alfano B, et al. Simplified, noninvasive PET measurement of blood-brain barrier permeability. J Comput Assist Tomogr 1987; 11:390–397.
15a. Ott RJ, Brada M, Flower MA, Babich JW, Cherry SR, Deehan BJ. Measurements of blood-brain barrier permeability in patients undergoing radiotherapy and chemotherapy for primary cerebral lymphoma. Eur J Cancer 1991; 27:1356–1361.
15b. Hawkins RA, Phelps ME, Huang SC, et al. A kinetic evaluation of blood-brain barrier permeability in human brain tumors with "^{68}Ga"DTPA and positron computed tomography. J Cereb Blood Flow Metab 1984; 4:507–515.
16. Yeung WTI, Lee TY, Del Maestro RF, Kozak R, Brown T. In vivo CT measurement of blood-brain transfer constant of iopamidol in human brain tumors. J Neurooncol 1992; 14:177–187.
17. Donahue KM, Weisskoff RM, Parmelee DJ, Callahan RJ, Wilkinson RA, Mandeville JB, Rosen BR. Dynamic Gd-DTPA enhanced MRI measurement of tissue cell volume fraction. Magn Reson Med 1995; 34:423–432.
18. Schwickert HC, Roberts TPL, Shames DM, et al. Quantification of liver blood volume: comparison of ultra short TI inversion recovery echo planar imaging (ULSTIR-EPI), with dynamic 3D-gradient recalled echo imaging. Magn Reson Med 1995; 34:845–852.
19. Yoshida K, Furuse M, Kaneoke Y, et al. Assessment of T1 time course changes and tissue-blood ratios after Gd-DTPA administration in brain tumors. Magn Reson Imaging 1989; 7:9–15.
20. Tofts PS, Kermode AG. Measurement of blood brain permeability using Gd-DTPA scanning. Magn Reson Imaging 1989; 7: 150.
21. Tofts PS, Kermode AG. Blood brain permeability measured in multiple sclerosis using labelled DTPA with PET, CT and MRI. J Neurol Neurosurg Psychiatry 1989; 52:1019–1020.
22. Tofts PS, Kermode AG, Barker G. Measurement of the blood-brain permeability using dynamic Gd-DTPA scanning. In: Proceedings of the 8th annual meeting of the Society of Magnetic Resonance in Medicine. Amsterdam: Society of Magnetic Resonance in Medicine, 1989; 805.
23. Larsson HBW, Stubgaard M, Frederiksen JL, Jensen M, Henriksen O, Paulson OB. Quantitation of blood-brain barrier defect using MRI and gadolinium-DTPA in acute multiple sclerosis. In: Proceedings of the 8th annual meeting of the Society of Magnetic Resonance in Medicine. Amsterdam: Society of Magnetic Resonance in Medicine, 1989; 744.
24. Larsson HBW, Tofts PS. Measurement of blood brain barrier permeability using dynamic Gd-DTPA scanning: a comparison of methods. Magn Reson Med 1992; 24:174–176.
25. Larsson HBW, Stubgaard M, Frederiksen JL, Jensen M, Henriksen O, Paulson OB. Quantitation of blood-brain barrier defect by magnetic resonance imaging and gadolinium-DTPA in patients with multiple sclerosis and brain tumors. Magn Reson Med 1990; 16:117–131.
26. Tofts PS, Kermode AG. Measurement of the blood-brain barrier permeability and leakage space using dynamic MR imaging: 1. Fundamental concepts. Magn Reson Med 1991; 17:357–367.
26a. Brix G, Semmler W, Port R, Schad LR, Layer G, Lorenz WJ. Parametrization of the MRI signal enhancement during and after i.v. infusion of Gd-DTPA: a pharmacokinetic model. In: Proceedings of the 9th annual meeting of the Society of Magnetic Resonance in Medicine. New York: Society of Magnetic Resonance in Medicine, 1990; 2:758.
27. Brix G, Semmler W, Port R, Schad LR, Layer G, Lorenz WJ. Pharmacokinetic parameters in CNS Gd-DTPA enhanced MR imaging. J Comput Assist Tomogr 1991; 15:621–628.
28. Kermode AG, Tofts PS. Non-invasive measurement of human blood-brain barrier transfer constant using dynamic magnetic resonance imaging. J Physiol 1990; 423:42P.
29. Weinmann HJ, Laniado M, Mutzel W. Pharmacokinetics of GdDTPA/dimeglumine after intravenous injection into healthy volunteers. Physiol Chem Phys Med NMR 1984; 16:167–172.
30. Tofts PS, Berkowitz BA. Rapid measurement of capillary permeability using the early part of the dynamic Gd-DTPA MRI enhancement curve. J Magn Reson (part B) 1993; 102:129–136.
31. Berkowitz BA, Tofts PS, Sen HA, Ando N, de Juan E. Accurate and precise measurement of blood-retinal barrier breakdown using dynamic Gd-DTPA MRI. Invest Ophthalmol Vis Sci 1992; 33:3500–3506.
32. Berkowitz BA, Wilson CA, Tofts PS, Peshock RM. Effect of vitreous fluidity on the measurement of blood-retinal barrier permeability using contrast enhanced MRI. Magn Reson Med 1994; 31:61–66.
33. Tofts PS, Berkowitz B. Measurement of capillary permeability from the Gd enhancement curve: a comparison of bolus and constant infusion injection methods. Magn Reson Imaging 1994; 12:81–91.
34. Tofts PS, Berkowitz B, Schnall M. Quantitative analysis of dynamic Gd-DTPA enhancement in breast tumours using a permeability model. Magn Reson Med 1995; 33:564–568.
35. Furman-Haran E, Margalit R, Grobgeld D, Degani H. Dynamic contrast enhanced magnetic resonance imaging reveals stress induced angiogenesis in MCF7 human breast tumors. PNAS 1996; 93:6247–6251.
36. Tofts PS. Optimal detection of blood-brain barrier defects with Gd-DTPA: the influences of delayed imaging and optimised repetition time. Magn Reson Imaging 1996; 14:373–380.
37. Boas ML. Mathematical methods in the physical sciences. New York: Wiley, 1966.
38. Larsson HBW, Christiansen P, Stubgaard M, Thomsen C, Frederiksen J, Henriksen O. In vivo calculation of the unidirectional influx constant across the blood-brain barrier using MRI. In: Proceedings of the 9th annual meeting of the Society of Magnetic Resonance in Medicine. New York: Society of Magnetic Resonance in Medicine, 1990; 2:752.
39. Larsson HBW, Stubgaard M, Sondergaard L, Henriksen O. In vivo quantification of the unidirectional influx constant for Gd-diffusion across myocardial capillaries with MR imaging. J Magn Reson Imaging 1994; 4:433–440.
40. Larsson HBW, Fritz-Hansen T, Rostrup E, Sondergaard L, Ring P, Henriksen O. Myocardial perfusion modeling using MRI. Magn Reson Med 1996; 35:716–726.
41. Fritz-Hansen T, Rostrup E, Larsson HBW, Sondergaard L, Ring P, Henriksen O. Measurement of the arterial concentration of Gd-DTPA using MRI: a step towards quantitative perfusion imaging. Magn Reson Med 1996; 35:225–231.
42. Diesbourg LD, Prato FS, Wisenberg G, Drost DJ, Marshall TP, Carroll SE, O'Neill B. Quantification of myocardial blood flow and extracellular volumes using a bolus injection of Gd-DTPA: kinetic modeling in canine ischaemic tissue. Magn Reson Med 1992; 23:239–253.
43. Burstein D, Taratuta E, Manning WJ. Factors in myocardial "perfusion" imaging with ultrafast MRI and Gd-DTPA administration. Magn Reson Med 1991; 20:299–305.
44. Deleted in proof.
45. Hoffmann U, Brix G, Knopp MV, Hess T, Lorenz WJ. Pharmacokinetic mapping of the breast: a new method for dynamic MR mammography. Magn Reson Med 1995; 33:506–514.
46. Buckley DL, Kerslake RW, Blackband SJ, Horsman A. Quantitative analysis of multi-slice Gd-DTPA enhanced dynamic MR images using an automated simplex minimisation procedure. Magn Reson Med 1994; 32:646–651.
47. Kuwatsuru R, Shames DM, Muhler A, et al. Quantification of tissue plasma volume in the rat by contrast-enhanced magnetic resonance imaging. Magn Reson Med 1993; 30:76–81.
48a. Su M, Jao J, Nalcioglu O. Measurement of vascular volume fraction and blood-tissue permeability constants with a pharmacokinetic model: studies in rat muscle tumors with dynamic Gd-DTPA enhanced MRI. Magn Reson Med 1994; 32:714–724.
48b. Gowland P, Mansfield P, Bullock P, Stehling M, Worthington B, Firth J. Dynamic studies of gadolinium uptake in brain tumors using inversion-recovery echo-planar imaging. Magn Reson Med 1992; 26:241–258.
49. Flickinger FW, Allison JD, Sherry RM, Wright JC. Differentiation of benign from malignant breast masses by time-intensity evaluation of contrast enhanced MRI. Magn Reson Imaging 1993; 11:617–620.
50. Heiberg EV, Perman WH, Herrmann VM, Janney CG. Dynamic sequential 3D gadolinium-enhanced MRI of the whole breast. Magn Reson Imaging 1996; 14:337–348.
51. Parker GJM, Tanner SF, Leach MO. Pitfalls in the measurement of tissue permeability over short time-scales using a low temporal resolution blood input function. In: Proceedings of the 4th annual scientific meeting of the International Society for Magnetic Resonance in Medicine. New York: International Society for Magnetic Resonance in Medicine, 1996; 3:1582.
52. Taylor NJ, Rowland IJ, Tanner SF, Leach MO. A rapid interleaved method for measuring signal intensity curves in both blood and tissue during contrast agent administration. Magn Reson Med 1993; 30:744–749.

53. Braunschweiger PG, Schiffer LM, Furmanski P. ^{1}H-NMR relaxation times and water compartmentalization in experimental tumor models. Magn Reson Imaging 1986; 4:335–342.
54. Donahue KM, Burstein D, Manning WJ, Gray ML. Studies of Gd-DTPA relaxivity and proton exchange rates in tissue. Magn Reson Med 1994; 32:66–76.
55. Shuter B, Tofts PS, Wang SC, Pope JM. The relaxivity of Gd-EOB-DTPA and Gd-DTPA in liver and kidney of the Wistar rat. Magn Reson Imaging 1996; 14:243–253.
56. PS Tofts, B Shuter and JM Pope. Ni-DTPA doped agarose gel: a phantom material for Gd-DTPA enhancement measurements. Magn Reson Imaging 1993; 11:125–133.